14.Site Characterisation

14.1 Introduction

Site characterisation is traditionally closely supervised by the institution in charge of the project with little or no input from the industry. Because each new astronomical development has particular site requirements. and because of the political and financial consequences of a site selection. inter-agency collaborations have been rather limited in the past. In the case of the ELTs however the picture has changed dramatically. mainly as a result of the apparition of new standards used in a decade of operational monitoring at the 8 meter class observatories. Site characterisation working groups have been setup to strengthen European (ELT-design study) as well as intercontinental (ESO-AURA) collaborations. Regular meeting take place (TMT workshops. IAU Site) which favour open-minded exchanges.

14.1.1 Instrumentation and methods

14.1.1.1 Cloudiness

Most institutions have developed all-sky cameras. in the visible or the infrared. with a 180 degree field of view which aim at visualising arriving clouds during telescope operation. Because of the poor optical quality of the fish-eye lens. there is currently no standard automated data processing which could be used for site characterisation. Both types of all-sky cameras (COBBER and ICECAM) were used by the Australian team in Antarctica Dome C and provided partial but valuable statistics before the first manned winter over was possible.

Statistics of photometric time on existing observatory still rely on the night reports written from visual inspections of the sky by the telescope operator. subject to post facto confirmation through analysis of calibration observations (photometric zero points). Most observatories follow a classical definition [44] of a photometric night. i.e. at least 6 night time hours in a row with sky clear down to 5 degree above horizon (night time is restricted to hours for which the sun has an attitude lower than 18 degrees below the horizon). On remote sites with some automated seeing monitoring. line of sight stellar photometry is used to estimate the amount of clear time.

On remote candidate sites without infrastructure. the analysis of satellite database described in 14.2.1.1. initially introduced by ESO [45] [46] [47]. is now used in a homogeneous way by most institutions [48] [49] [50]. The method is however limited by temporal under sampling (one image every 3 hour only) and variability of ground thermal footprints. Moreover. local perturbations like fog are not detected. Cross-calibration of the method with data from photometric surveys (2MASS) took place recently in the frame of the LSST site selection process [51]. It concluded that there is a maximum of 8% misses in Southern US. less than 2% in Northern Chile.

14.1.1.2 Precipitable Water Vapor

Specific PWV detectors have been developed in the 80's for the optical (IR sky monitor) and radio (Tipper) projects. The latter measures optical depth and conversion to PWV rely on an atmospheric model which limits the cross-calibration performance. Tippers are in use in Hawaii and South Pole and were a major tool in the selection of the ALMA site of Chajnantor.

Satellite measurements can be used to assess PWV and the method was successfully cross-calibrated [45] at Paranal with the IR sky monitor used during the VLT site survey. giving an rms error of 1mm H2O. On very dry sites like Chajnantor. the satellite method reaches critical limits. An attempt to compare to tipper data at Chajnantor [48] gave encouraging results but also raised questions which prompted a re-analysis of the tipper data. work is underway. On the other hand. satellite based PWV data produced regularly for La Silla are currently questioned by the Campanas team and a joint cross-calibration campaign is planned using spectroscopic observations as well as a newly developed IR sky monitor (IRMA) in operation at Cerro Pachon.

14.1.1.3 Aerosol Extinction

Normally measured from the ground using astronomical photometry (Geneva Observatory for La Silla. CAMC for La Palma). for instance the long term effects of major volcanic eruptions were accurately tracked from the ground. Large changes in atmospheric extinction can also be monitored from UV satellite observations. It was demonstrated for instance [52] that events of contamination of the Canarian and Moroccan sky by the Saharan dust could be extracted from the TOMS satellite records.

Other sources of sporadic extinction are the condensed trails (contrails) left by commercial jets along the main corridors over low populated areas normally chosen for their dark skies. Typically contrails can only form at temperatures below negative-76 degrees Fahrenheit and at humidity levels of 70 percent or more at high altitudes. Most contrails occur during the winter months and least during the summer [71]. Although nocturnal observations are not available. it appears that the contrails have a diurnal variation that peaks during mid morning over most areas. A significant correlation exists between mean contrail frequency and aircraft fuel usage above 7 km suggesting predictive potential. Projections for 2050 are available of the increase of the overall yearly traffic (see 14.2.1.3.2). but no distinction is made between day and night time. Such a distinction would be relevant for optical astronomy since in most common situations a jet contrail lasts no more than 30 minutes although it was observed that some of them linger for hours and actually become clouds.

14.1.1.4 Seeing

Most observatories are now equipped with the same kind of seeing monitor. based on the differential image motion method (DIMM) [61]. complemented by [62] and [63]. Because the method is rather robust. and provided no particular filtering of individual images was performed. the data obtained by thus monitors on various sites are comparable. The height above ground at which the measurements took place should be carefully analyzed because the depth of the ground thermal inversion layer is highly variable from site to site.

14.1.1.5 Turbulence Vertical Profiles

The complete profile of the turbulence along the optical path is only accessible by the SCIDAR technique which requires a telescope diameter larger than one meter is not applicable to remote sites. A portable version. the Single Star SCIDAR is currently under development at Nice University under FP6 ELT Design Study. Complete profiles are also obtained by balloon borne microthermal sensors. however drifting far away from the launching place in the course of their ascent. The balloon profiles present low statistical significance for site comparison but they are however extremely useful as input for the adaptive optics numerical modelling [68].

Turbulence in the surface layer (the first tens of meter above the ground) is best measured by microthermal sensors attached on a mast. following the technique mastered by Nice University [64] and in use everywhere. Attempts to use commercial and more robust sonic anemometers are underway.

Turbulence in the so-called ground layer (the first kilometre above the ground) is the most difficult to monitor accurately. Acoustic sounders (SODAR) used in various places did give interesting qualitative information but lack accuracy. More recently the SLODAR [58] [59] technique was introduced by Durham University and a currently unique portable version was developed for ESO Paranal monitoring (see 14.2.3.1) [60].

Turbulence above 1km is well monitored using the successful MASS instrument from Sternberg Institute Moscow [65]. the development of which was co-funded by ESO and CTIO. More than 10 such devices are now in operation around the world. one at ESO Paranal where the consistency of the MASS integral profile with DIMM records is excellent (see 14.2.3.2). The MASS was recently compared to SCIDAR during a few nights at Mauna Kea observatory [66] showing a good agreement in the higher layers but misplacement by MASS of the lower turbulence.

14.1.1.6 Turbulence Outer Scale

One single instrument is capable of measuring the outer scale of the turbulence. The GSM was developed by Nice University with ESO funding and the first data were obtained in 1997 at La Silla [67]. Since then. the GSM instrument has been visiting most large observatories and a consistent database is available.

14.1.1.7 Wave front coherence time

Only the balloons give an accurate value for the coherence time since they provide both wind and turbulence profiles [70]. however averaged during the 1 hour flight duration. There is no standard for permanent wave front temporal coherence monitoring but some methods are at reach. Computer intensive algorithms allow the SCIDAR to retrieve the velocity of the layers it has detected. The MASS is routinely estimating the global coherence time of the high altitude layers. The DIMM. associated to forecasts of wind velocity at the tropopause is providing a reasonable estimate of tau0 and theta0. the isoplanatic angle [69].

14.2 Parameters space

14.2.1 General astronomy

14.2.1.1 Cloudiness

Even nowadays. statistics of photometric nights at many observatories are compiled by trained telescope operators visually inspecting the sky anytime there is some doubt. Useful tools such as all-sky cameras are available but do not yet provide a reliable accounting of non-photometric events under the very demanding astronomical criteria.

The cloudiness is routinely monitored and forecasted at ESO La Silla and Paranal Observatory since 1999 using 3-hourly satellite imagery in the 10.7 and 6.7 micron. channels [46]. The general hit rate is considered as satisfactory; however there is each year several reports of misses when the clouds are either short lived or extremely thin.

It is of course tempting to derive photometric night statistics over any candidate site from satellite imagery using the same method as [49] in the frame of the TMT site survey. However caution is recommended when comparing sites in different climatic zones and with particular seasonal events (e.g. monsoon. Bolivian winter). Analysis of satellite data at 6.7µm and 10.7µm for Mt Hopkins has shown that the satellite-derived clear fraction for the site (56.6%) is similar to that determined for Kitt Peak (59.4%) in an earlier study using identical methodology [49]. As stated in a study for the LSST project [50]. the photometric fraction determined for Mt Hopkins by 2MASS (43.2%. adjusted) is significantly lower than the satellite clear fraction. Differences in methodology may account for about half of the observed difference. Using a time-based method

to determine the satellite clear fraction that is computationally similar to the method used to derive the 2MASS photometric fractions. the difference between the satellite and 2MASS clear/photometric fractions is reduced to about 8%.

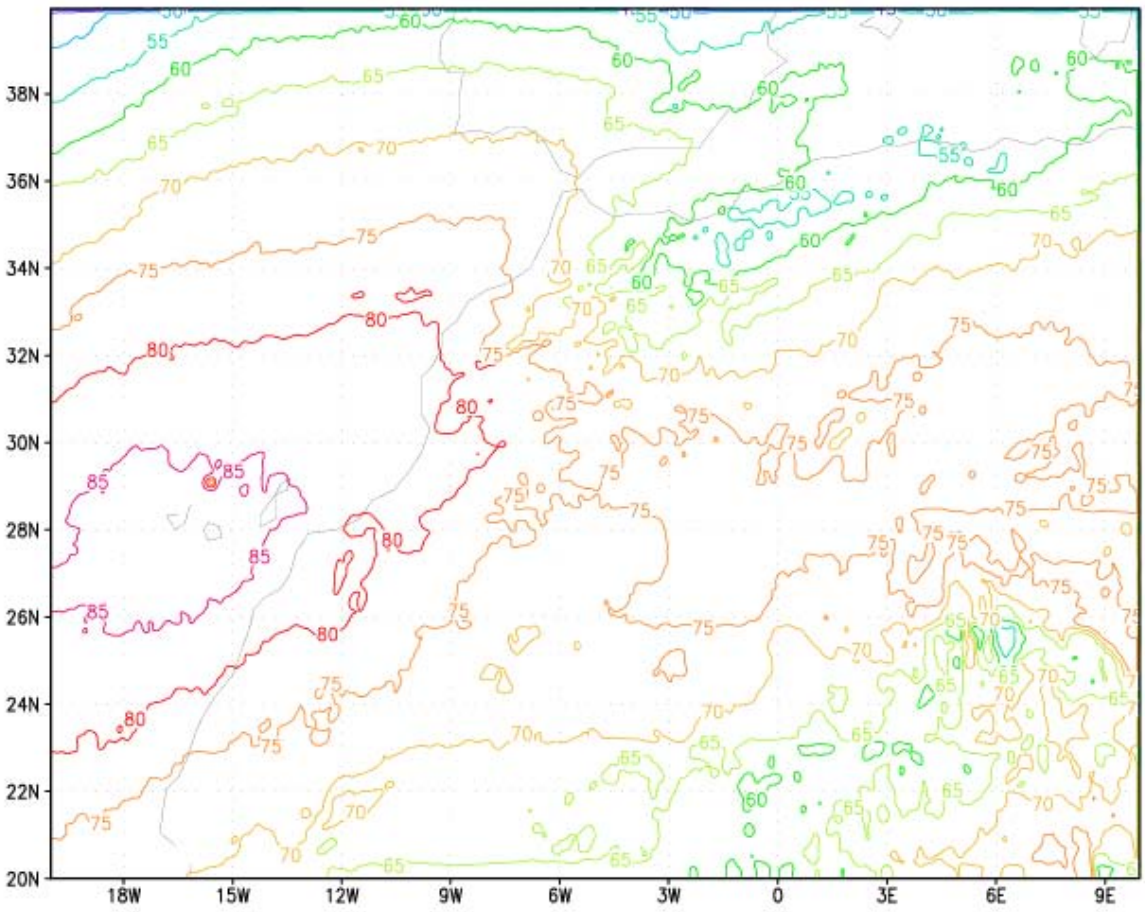

Figure 14-1: Fraction of time that skies are clear (%) at night for the years 1999 and 2000 over Canaries. NW Africa and Southern Spain (A. Erasmus. ESO Interim Report. Oct. 2004)

Nevertheless. the method can be used with confidence in relative terms. for optimizing the site selection within one area. In particular. the preliminary results of an ongoing 7-year survey have shown (Figure 14-1) the superiority of the Anti-Atlas summits over any others within the Moroccan territory. It is interesting to note on this diagram that. from the point of view of the general circulation. the Canary Islands appear as the best location over the whole studied area. Of course. the relatively low spatial resolution (10km) of the analysis does not allow taking into account local phenomena such as the Caldera effect.

14.2.1.2 Precipitable water vapour

Several studies [46]. [47] have shown that it was possible to accurately measure precipitable water vapour from satellite imagery in the 6.7 micron water vapour channel. A comparison of the results with ground based measurements at Paranal and Chajnantor (Table 14-1) have shown that the method could be accurate within 10% even in the driest sites. The PWV observing conditions are routinely monitored at Paranal since 1999 and forecasts are produced every three hours for the next 36h.

Site	Paranal		Chajnantor	
Sensor	Satellite	Site Monitor	Satellite	Site Monitor
Period	Day	Night	Day	24 hrs
10th percentile	1.83	1.70	0.30	0.26
1st Quartile	2.57	2.41	0.47	0.40
Median	4.05	3.66	0.72	0.77
3rd Quartile	7.27	5.21	1.26	2.16

Table 14-1: PWV (mm) statistics for Paranal (January - August 1998) and Chajnantor (January - September 1999) for satellite and ground based site monitor measurements of PWV.

The same method can be advantageously applied to site selection in areas which are not equipped with ground based monitoring. As an example a study by Erasmus [48] allowed to rank several candidate sites in NW Argentina. Northern Chile and Southern Bolivia (Figure 14-2).

No	Site	Latitude	Longitude	Size (kmxkm)	Altitude (m)	Max altitude
1	Chajnantor	-22.983	-67.629	10 x 10	5000	5639
2	Chalviri	-22.508	-67.716	10 x 7	5200	5780
3	Arg High	-25.065	-66.945	4 x 3	5100	5355
4	Arg Mid	-25.385	-66.746	8 x 5	4900	5163
5	Arg South	-26.540	-67. 887	10 x 6	4900	5308
6	Arg Low	-24.073	-67.434	> 10 x 10	4400	5665
7	Arg West	-25.171	-68.313	4 x 4	5200	5400

Table 14-2: Site locations and information

The 6.7µm (water vapor) and 10.7µm (IR window) satellite imagery used in this study are from the International Satellite Cloud Climatology Project (ISCCP) data set. Five years of satellite data covering the period July 1. 1993 to February 28. 1996 and June 1. 1997 to August 31. 1999 were purchased from the U.S. National Climatic Data Center (NCDC) by Cerro-Tololo Inter-American Observatory (CTIO) and University of Tokyo (UT). A data use agreement between these parties and ESO facilitates the use of these data for this study.

The results given in Figure 14-3 confirmed the superiority of Chajnantor. the ALMA site. over other candidates of similar altitude. Only one higher site in Southern Bolivia came out slightly better.

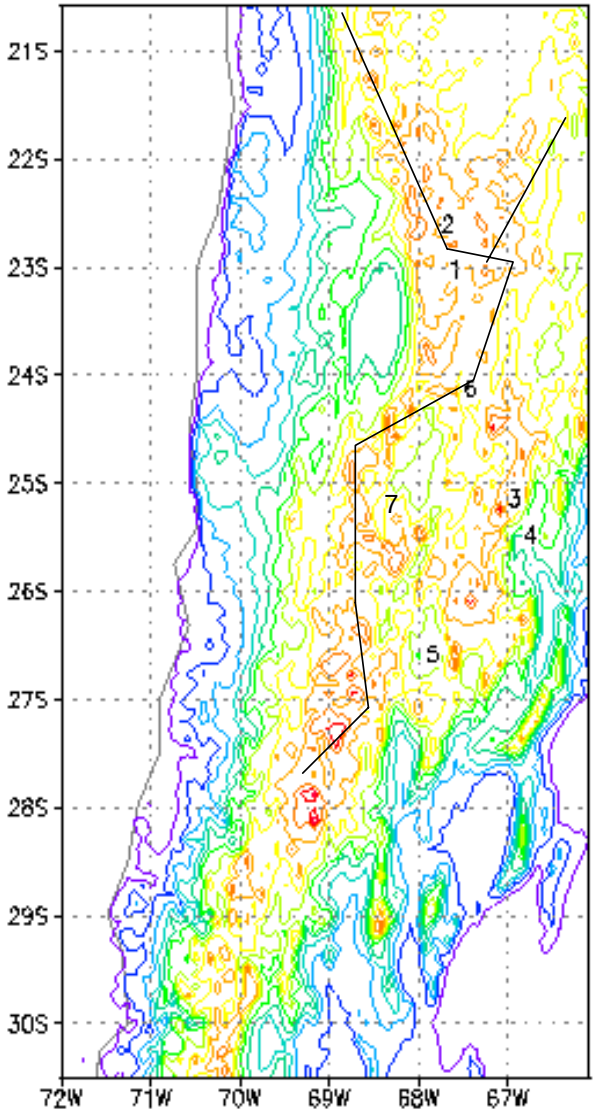

Figure 14-2: Locations of the sites in Chile. Bolivia and Argentina that were compared using satellite data. Contours show the topography at 500m intervals (see Table 14-2).

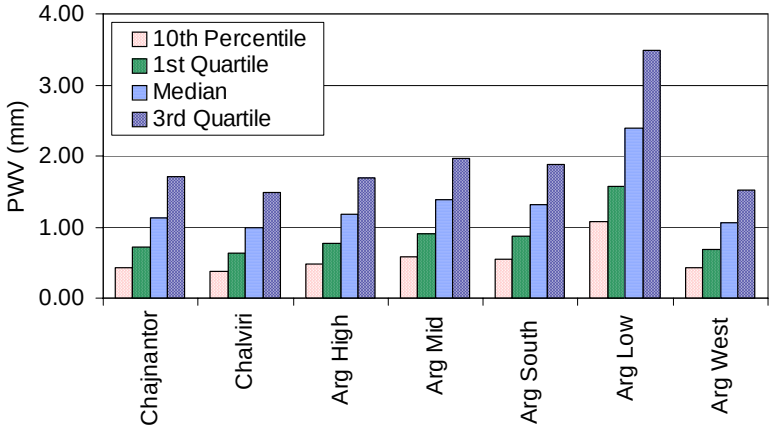

Figure 14-3: PWV percentile values at each site under clear conditions.

14.2.1.3 Aerosol Extinction

14.2.1.3.1 Saharan dust

Based on a comparison of extinction measurements made in the optical by CAMC at ORM Observatory (Figure 14-4). it has been demonstrated by Siher et al. that the events of contamination of the sky transparency by airborne aerosols could be detected from satellite observations in the UV.

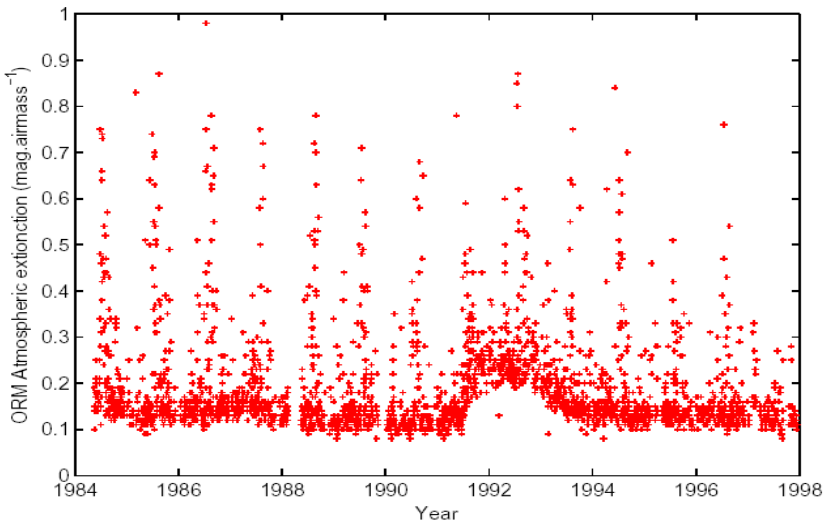

Figure 14-4: The Carlsberg Meridian Circle (CAMC) database at La Palma

As shown on Figure 14-5. the extinction coefficient at 680 nm divided by its sigma value presents a sharp slope change at K680=0.075 (K550~0.15). Siher et al. choose conservatively K550>0.2 for CAMC threshold of non photometric sky.

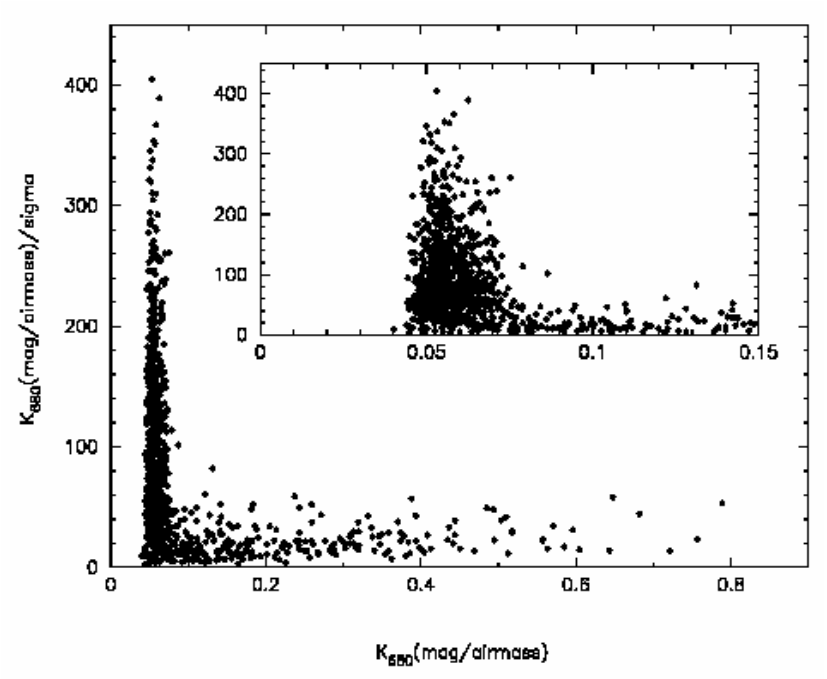

Figure 14-5: Diurnal Atmospheric Extinction over Teide Observatory (Tenerife. Canary Islands). Ref: A. Jimenez et al.. Fig.4

Using this threshold. it was shown that satellite data above a given optical depth were reasonably well correlated (Figure 14-6). Hence a UV satellite database was added to the FRIOWL site selection tool described in 14.3.3.2.

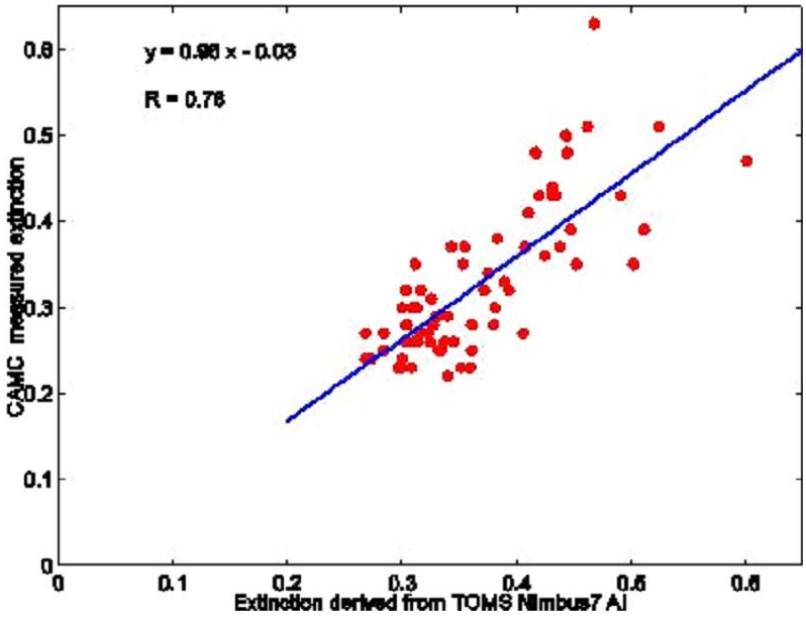

Figure 14-6: Correlation of satellite UV and ground based V monthly averaged measurements CAMC AE>0.20. NIMBUS7 AE>0.2. Pixel center < 55km from ORM

14.2.1.3.2 Contrails

The projections for OWL mid-life of the contrail coverage shown on Figure 14-7 are indeed very alarming for astronomy. mainly for daytime observations. Individual candidate sites should be examined carefully to assess the expected nocturnal contamination. Contrail formation from jet exhaust is much less probable at night and the traffic is mostly limited to inter-continental flights.

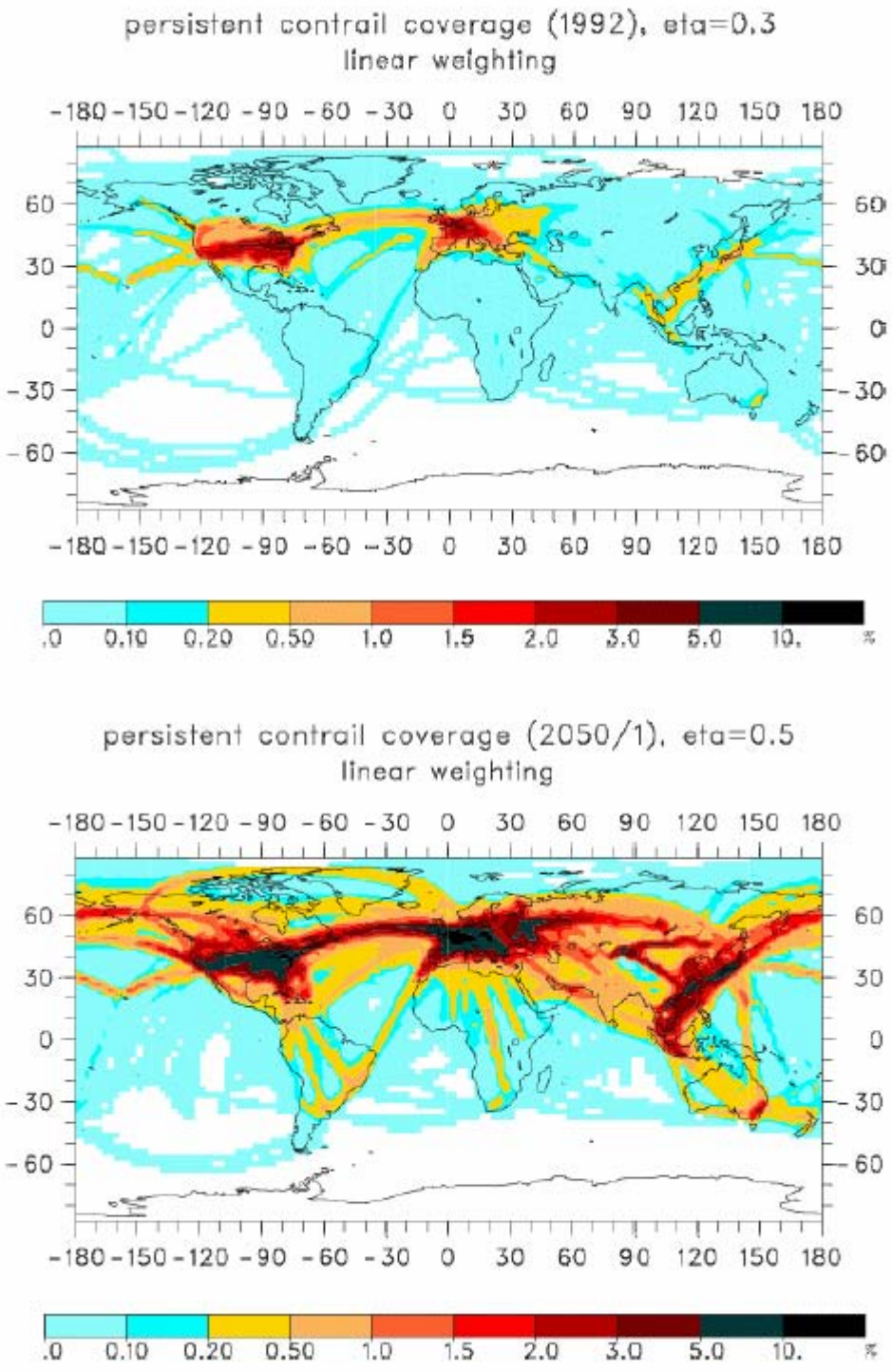

Figure 14-7: World map of jet aircraft contrails in 1992 (top). and predicted for 2050 (bottom). from [72]

14.2.1.4 Sky background

The sky background was not measured at Paranal during the VLT site survey. with the exception of the water lines used for the PWV monitoring. It was thus not part of the parameter space. with the assumption that no reason could be found that it would be worse than at La Silla. already considered as a very dark site. Accurate estimates of such a wavelength dependent parameter. which can only be obtained from analyzing science data. were made available one decade later. confirming the excellent quality of the site (Table 14-3 and Table 14-4).

Band	J	H	Ks	L	M-NB
Magnitude	16.5	14.4	13.0	3.9	1.2

Table 14-3: Typical IR Backgrounds at Paranal (mag/arcsec-2). from J. Cuby et al.. The Messenger 101. p.3. September 2000. Note that K. L and M values include telescope background.

Band	U	B	V	R	I
Magnitude	22.28	22.64	21.61	20.87	19.71

Table 14-4: Average background at Paranal (mag/arcsec-2). from >4000 FORS1 exposures during Apr.-Sep. 2001. by F. Patat. UBVRI Night Sky Brightness at ESO-Paranal during sunspot maximum. *The Messenger 115. March 2004.*

The light contamination of the visible sky background by public lighting is of course a concern for all major observatories sited at less than 100 km of urban areas. The efforts developed by ORM at La Palma as well as by CTIO in Chile have shown that it is possible. by proper legislation. to maintain the contamination at an acceptable level without impeding the economic development of the region. This has of course some limits (Palomar. Kitt-Peak) when mid-size cities turn into megalopolis. A clear projection of the expected economic development of each candidate over the expected lifetime of the observatory is thus required.

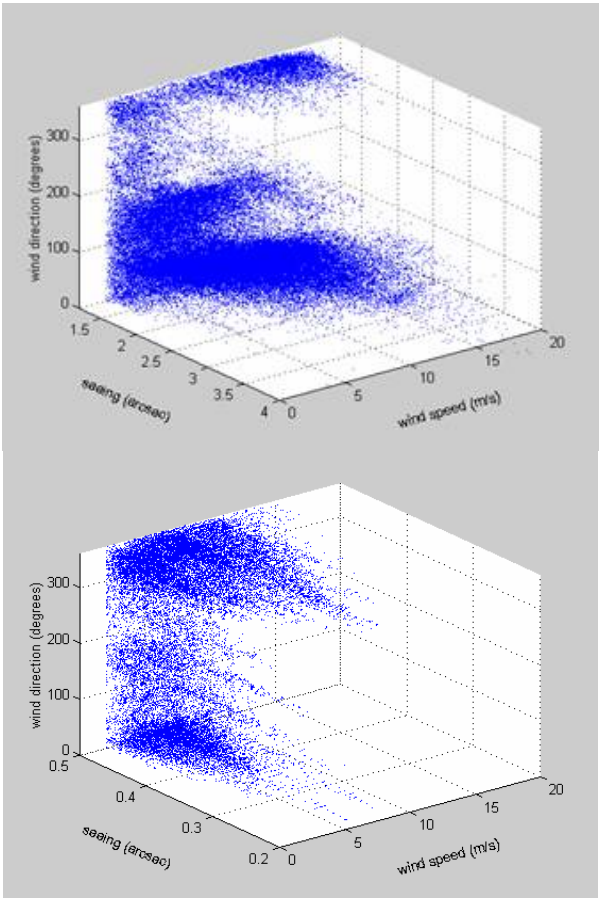

Figure 14-8: Seeing vs. local wind direction (0=North. 90=East etc.) and velocity at Paranal for best (right) and worst (left) observing conditions (2001-2004. over 778127 samples; J. Navarrete. ESO Observatory)

14.2.1.5 Seeing

The seeing is the result of the interaction of light with the numerous turbulence layers existing in the atmosphere above the site. Detailed vertical turbulence profiles described in 14.2.3 show that a large part of the turbulence is concentrated in the lower atmosphere. It is thus very useful.

as shown on Figure 14-8. to compare seeing records with local wind measurements to detect site related features which in turn shall be used to optimize telescope design and operation. It can be seen that the best seeing is obtained at Paranal for moderate wind (5m/s) coming from the North and North-West while the worst conditions are brought by strong winds (15m/s) from the North-East.

14.2.2 Telescope design & operation

14.2.2.1 Wind. temperature and humidity

Operation limits for an ELT are similar to those currently applied for the 8 to 10 meter class telescopes. However the emergency procedures are much slower to complete on extremely large structures. As an example. rolling the enclosure over the OWL telescope takes 30 minutes while a VLT Unit Telescope can be protected from rain or condensing clouds in a matter of a few minutes only. The consequence for OWL site survey is that the available clear time estimated for a given site cannot be a simple arithmetic addition of the periods when none of the meteorological parameters exceed the limits for observing conditions. The distribution in time of meteorological events shall be studied in detail and realistic strategy for emergency procedures shall be simulated.

14.2.2.2 Seismicity

Seismic hazard is basically the degree of earthquake shaking that one can expect in a given place during a given time. The map on Figure 14-9 is computed for solid rock and relatively fast shaking (0.2 second period). which strongly affects ordinary buildings.[68]

Different ground and different periods are important in determining the exact seismic *risk* for a particular structure. In the case of ELT's. and especially for the largest sizes. the structural design requires a substantial effort to cope with stresses caused by earthquakes. also because the order of magnitude of the eigen frequencies of the telescope structures falls into the region where the seismic response spectrum is the highest (2 to 6 Hz).

For this reason the seismic activity of a site. in terms of ground peak acceleration. is an important parameter which may decide whether an ELT can or cannot be built on that specific site. As shown in Table 14-4. these values make of Mauna Kea a site with a risk of seismic activity comparable to the one of Paranal. In particular a detailed study conducted for the Gemini project (Dames & Moore. 1994) concludes to a 10% exceedence probability in 50 years 20% higher at Mauna Kea than at Cerro Pachon. the Chilean site of Gemini South.

Site	Acceleration (g)
Mauna Kea	0.40
Paranal	0.34
La Silla	0.30
La Palma	0.06

Table 14-5: 50-years horizontal ground peak acceleration (g units) with 10% probability of exceedence.

[68] See also http://geology.about.com/library/weekly/aa010900a.htm.

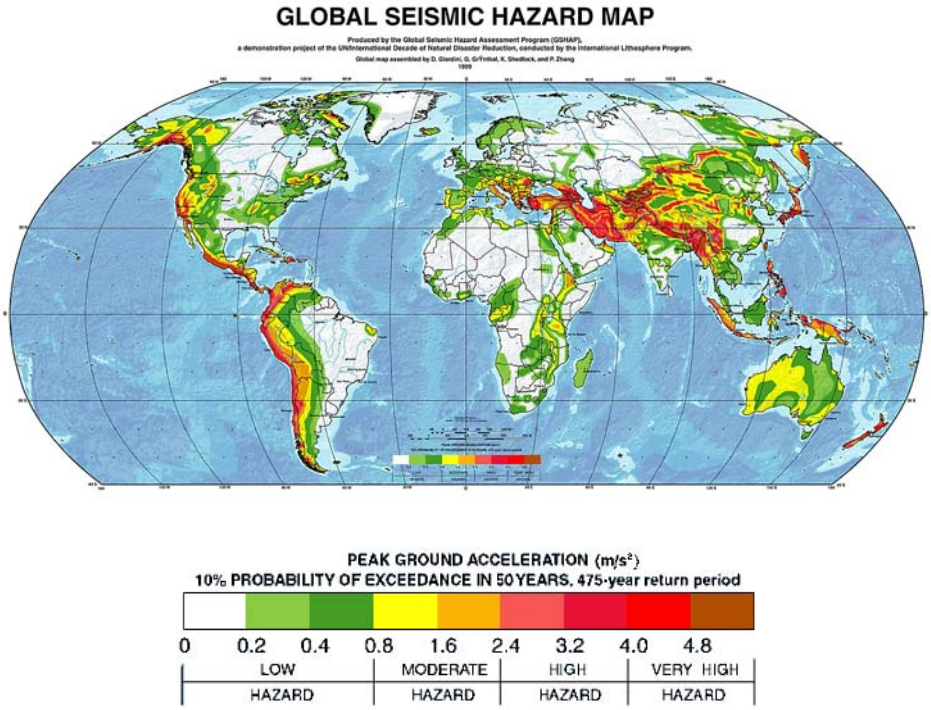

Figure 14-9: Peak ground acceleration (PGA) that a site can expect during the next 50 years with 10 percent probability GSHAP (Global Seismic Hazard Assessment Project)

14.2.2.3 Topology. soil characteristics

The extension of the site to accommodate the telescope platform of OWL is in the order of about .4 km^2 (about 34 football pitches). Foundations for the enclosure day and night parking positions and for the sliding system plus the foundations of the telescope will extend on a good part of the flattened area as shown in Figure 14-10.

The conceptual design has foundations which reach the maximum depth of about 30m from the level 0 of the flattened site. Moreover the design of the foundations has been carried out using site soil characteristics which assume compact ground and homogenous soil. therefore not including provisions for large consolidation works or large concrete works to build interconnected foundations. relying on the soil homogeneity.

The site survey shall start from the topology. Sites presenting large flat areas at the top of the mountain should be preferred for what concern civil work constraints. Quite extensive geotechnical tests shall be carried out on the site to gather the knowledge on its quality.

Following what was done for VLT the following tests should be performed:

- Density
- Unconfined compressive strength
- Point load strength
- Static elastic Young modulus
- Dynamic elastic Young modulus
- Shear modulus
- Poisson ratio
- Rock Quality Designation (RQD) via boreholes
- Status of soil fractures via sound propagation speed measurements.

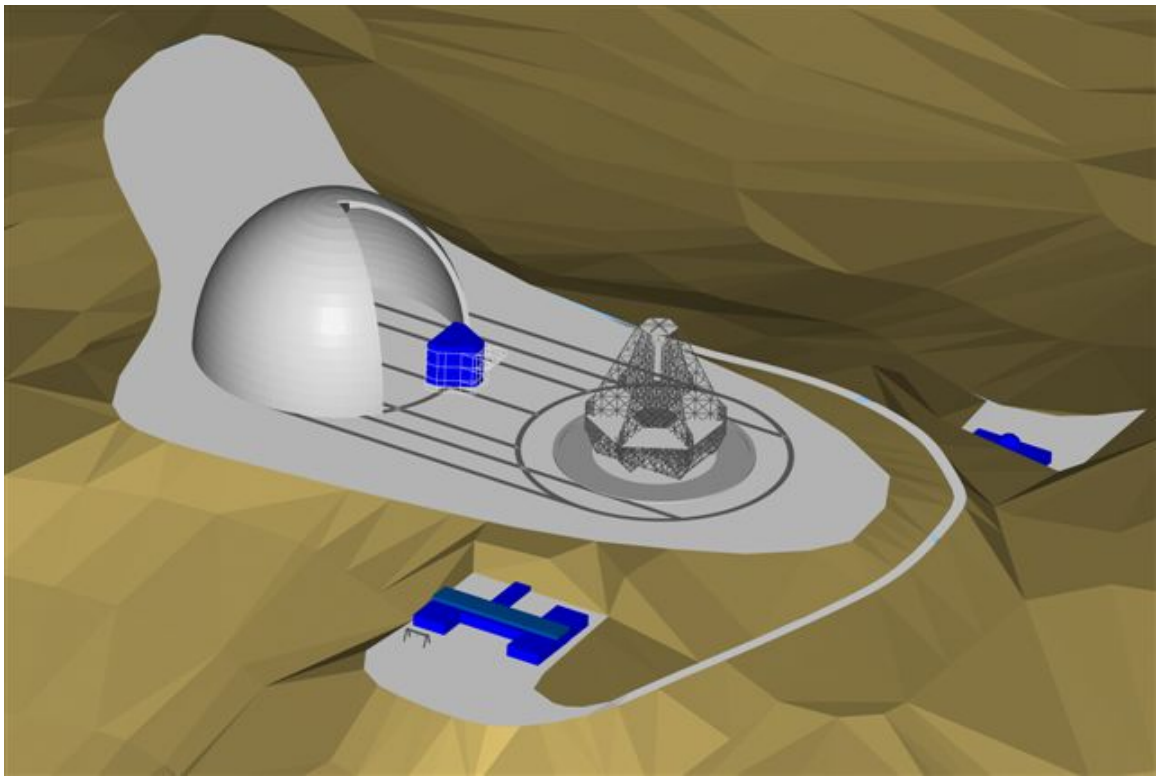

Figure 14-10: Site view

In Table 14-6 the characteristics measured for Paranal. also used to study the site of Paranal-North (Ventarones). and La Palma are summarised. Electrical resistivity of the soil should also be measured to assess the capability of a site to dissipate currents for equipment grounding purposes.

	Site I	**Site II**
Classification of soil according to EUROCODE 8 (defined by sound propagation speed (class A corresponds to waves speed propagation higher than 800 m/s)	A	A
Density [t/m^3]	2.7	2.6
Unconfined compressive strength [MPa]	98	20
Point load strength index (Is) [MPa]	9.8	2
Young modulus static [MPa]	10000	1100
Shear modulus static [MPa]	3800	430
Young modulus dynamic [MPa]	45000	5400
Shear modulus dynamic [MPa]	17500	2100
Poisson ratio	0.27	0.29

Table 14-6: Soil characteristics for Paranal area (Site 1) and La Palma (Site II)

14.2.2.4 Infrastructures

The dimension of the enclosure of OWL has some impact on the requirements that the site must have and on the equipment which must be installed to forecast meteorological events. The emergency shut down procedure takes 30 minutes until the telescope if fully protected. Moreover the enclosure can be moved with a wind speed as high as 27 m/s. These two characteristics imply the following:

- A meteorological station shall be in place which assures that the emergency shut down procedure starts at least half an hour before rain or other events start.
- Some modelling of the wind speed time gradient must implemented to start emergency shut down procedure at least half an hour before the wind exceeds 27 m/s.
- Possible need of further meteorological stations at different locations at several km from the site.

The other infrastructures of OWL do not present special demands on the site.

The distance from harbours qualified to handle large payloads. and to infrastructure like power network. drinkable water sources. industry for procuring supplies and services. should also come into the list of site requirements. although always subsidiary to astronomical parameters.

14.2.3 AO observations

14.2.3.1 Lower atmosphere turbulence and wind

A prototype portable seeing and turbulence monitor based on the SLODAR method was developed for ESO by R. Wilson from the AIG Durham[69]. The system comprises a Meade 40cm telescope equipped with an 8x8 element Shack-Hartmann WFS (5cm sub-apertures). The turbulence altitude profile is recovered from the time-averaged spatio-angular cross-correlation of the instantaneous wave front slopes. measured in the telescope pupil plane by using a Shack-Hartmann wave front sensor to observe a bright binary star. A vertical resolution of about 1.5km could be achieved for observations of narrow (5-7") binary stars (SLODAR-NB) and down to 150m when observing wide binaries (55-60"). Exposure times of the order 1-2 milliseconds are required in order to 'freeze' the seeing-induced motions of the WFS spots on 5cm apertures. placing strict requirements on the detector system. In order to achieve continuous monitoring. a limiting magnitude of V~7 for individual binary components is required to provide sufficient target stars. A detector with high QE. and read-out noise less than 1 electron rms is necessary. A camera based on the new E2V L3Vision CCD technology[70]. such as the Andor Technology iXon CCD cameras[71]. meet these requirements.

In Figure 14-11. the binary star projects 'copies' of the wave front aberration produced by the turbulent layer at altitude H onto the ground. with separation S. Hence there is a peak in the slope cross-correlation function for spatial offset S. H can be found by triangulation. given the binary star separation angle (theta). The strength of the layer is related to the amplitude of the cross-correlation signal (Figure 14-13). The full normalized profile is recovered from the cross-correlation via a de-convolution. where the autocorrelation of the wave front slopes for a single star of the binary is used as a measure of the (altitude-independent) impulse response of the system to a single turbulent layer. Although the cross-correlation is in two dimensions. we need only consider a cut through the function in the direction of the binary star separation. The total integrated turbulence. quantified by Fried's parameter r0. is found from the variances of the Zernike aberration terms for the centroid data (Figure 14-12).

[69] http://www.eso.org/astclim/paranal/asm/slodar/

[70] http://e2vtechnologies.com/introduction/prod_l3vision.htm

[71] http://www.andor-tech.com/

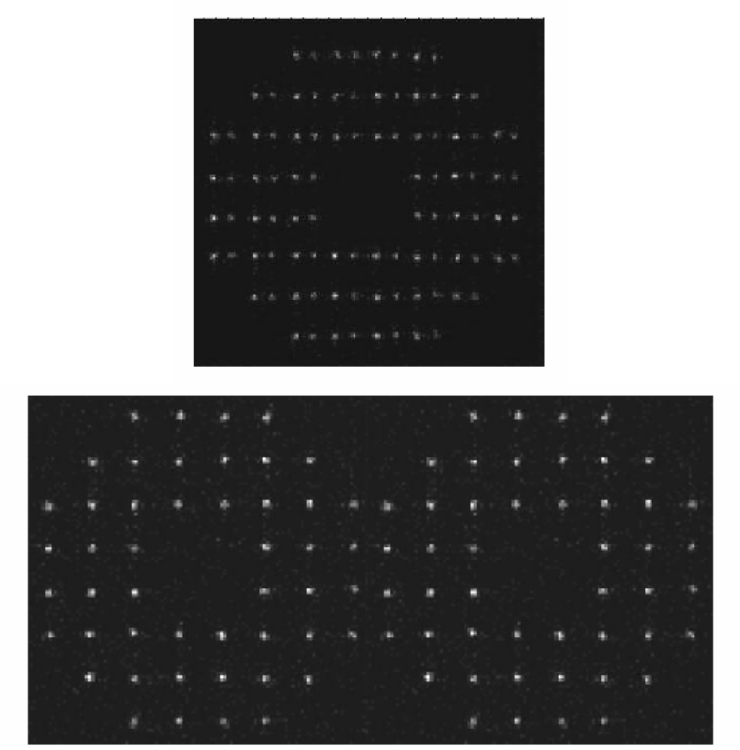

Figure 14-11: SLODAR Shack-Hartman pattern using narrow (left) and wide (right) binaries.

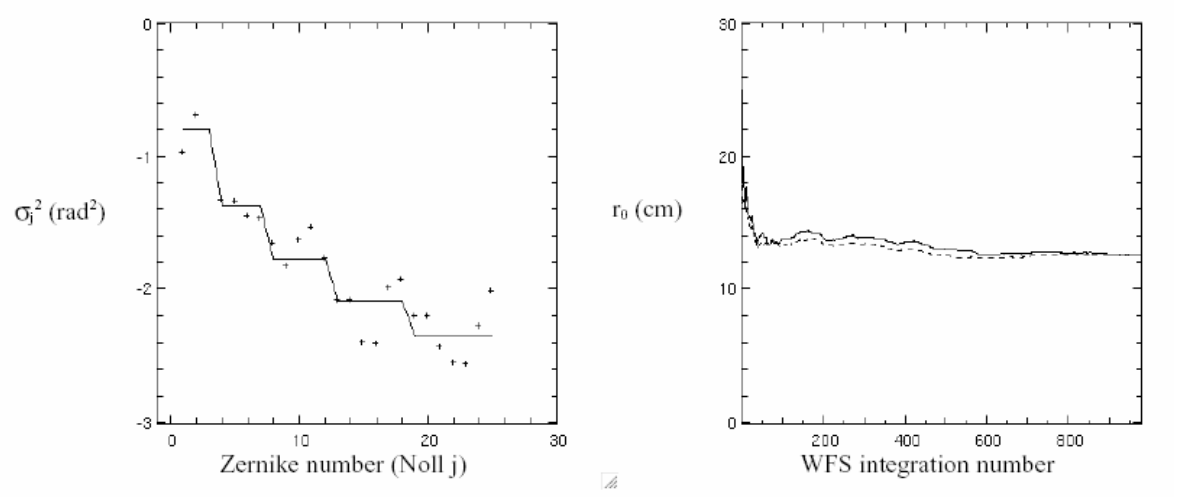

Figure 14-12: An example SLODAR determination of r0. Left: Measured Zernike coefficient variances. σj (crosses) and the theoretical (Noll) fit (solid line). Right: Calculated value of r0 versus WFS integration number (2ms CCD integrations at 190Hz)

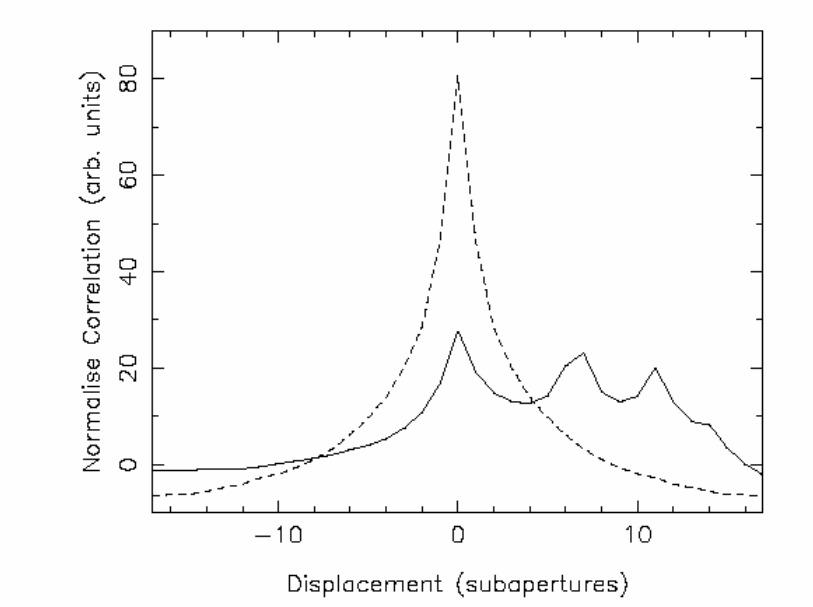

Figure 14-13 One-dimensional simulated cross-correlation (solid line) and autocorrelation (broken line) in the direction of the binary separation for a 24x24 sub-aperture.

Critical Data Analysis:

1. The altitude resolution of SLODAR depends on the separation of the selected binary and on the zenith angle. Thus for a given target. the altitudes of "layers" change with time. following the cos(z) law.
2. The SLODAR is at ground level. In case of very good seeing. the contribution of the first meters above ground is not negligible anymore compared to DIMM which is at 5m height. Note that the non-moving internal turbulence has been removed by temporal filtering.
3. The SLODAR has provisions to assess the wave front speed by temporal correlation of consecutive exposures. This function is however not yet implemented in the portable version.

14.2.3.2 Higher atmosphere turbulence and wind

MASS (Multi Aperture Scintillation Sensor) is a small instrument to measure vertical turbulence profile (http://www.ctio.noao.edu/~atokovin/profiler/). Unlike previous techniques. it is simple and inexpensive. destined to work continuously as a turbulence monitor at existing and new sites. MASS is based on a statistical analysis of stellar scintillations in four concentric ring apertures.

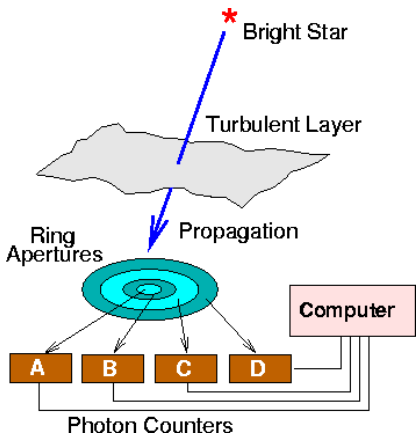

Figure 14-14: MASS principle. scintillation of a single star is measured through 4 concentric annular apertures.

This novel approach was proposed in 1998 and tested the same year at Mt. Maidanak in Uzbekistan (Kornilov. 2001). The first MASS instruments came into operation in 2002 at Cerro Tololo. It were built by a team at the Sternberg Astronomical institute (Moscow) led by Victor Kornilov under AURA and ESO contracts (Tokovinin. 2003). The control software provides on-line data reduction. so one can watch the turbulence evolution on a computer screen in real time.

The vertical resolution of MASS is low. only about 1/2 of altitude. The whole atmosphere is subdivided into 6 thick slabs (.5. 1. 2. and 4. 8 and 16 km) and the turbulence intensity in each layer is measured. Ground-layer turbulence does not produce any scintillation; it is not sensed by MASS. On the other hand. DIMM senses the whole atmosphere. Turbulence intensity in the ground layer can be found by combining MASS and DIMM data: the two instruments should always work together. For that purpose a combined MASS-DIMM pupil segmentator was developed where the same telescope feeds both instruments: two apertures are sent to the DIMM channel whereas four concentric apertures are cut to feed the MASS detectors.

Critical Data Analysis:

a) The integral characteristics of turbulence are measured by MASS quite reliably. However. the profile restoration is delicate; hence sometimes turbulence is attributed to wrong layers. The restoration errors are largest in the lowest (0.5km) layer. most important for GLAO.

b) MASS restoration is based on linear theory applicable to very weak scintillation. It was found that MASS systematically over-estimates the turbulence integral ("overshoots") when the scintillation index exceeds ~0.1. A first-order correction to overshoots. found by numerical simulations. is applied to the MASS data. However. in some cases (notably for fast turbulence) some residual over-shoots may remain. In this case the ground-layer turbulence estimated from DIMM minus MASS is under-estimated.

c) MASS is delivering estimates of the wave front coherence time based on the temporal spectrum of the scintillation. The comparison of MASS derived coherence time with estimates from combining DIMM seeing and 200 mb wind speed [69] show a very good agreement only during part of the time. A second regime exists when MASS and DIMM coherence time disagree. the nature of which is under investigation.

14.2.3.3 Full Atmospheric profiles

It is possible to combine contemporaneous SLODAR and MASS measurements to reconstruct the relative contribution of each of the layers sensed by the two instruments (Figure 14-15). Taking into account their respective thickness of integration. the complete atmospheric profile reduced to zenith can then be reconstructed (Figure 14-16) to be used as input for adaptive optics simulation purposes.

The deployment of MASS devices on all candidate sites is foreseen within the frame of the ELT-FP6 Design study (WP 12200). SLODAR. on the other hand exists as a unique transportable prototype.

An alternative system. also funded by the ELT-FP6 Design study is currently developed at Nice University: a Single Star SCIDAR (SSS) profiler which could make use of small size telescope down to 40cm. Compared to the classical SCIDAR which uses double stars and large (>1m) telescopes. the SSS would have the advantage of portability. at the cost of a lower altitude resolution. Moreover. the SSS would be able to monitor the velocity and direction of motion of all resolved turbulence layers.

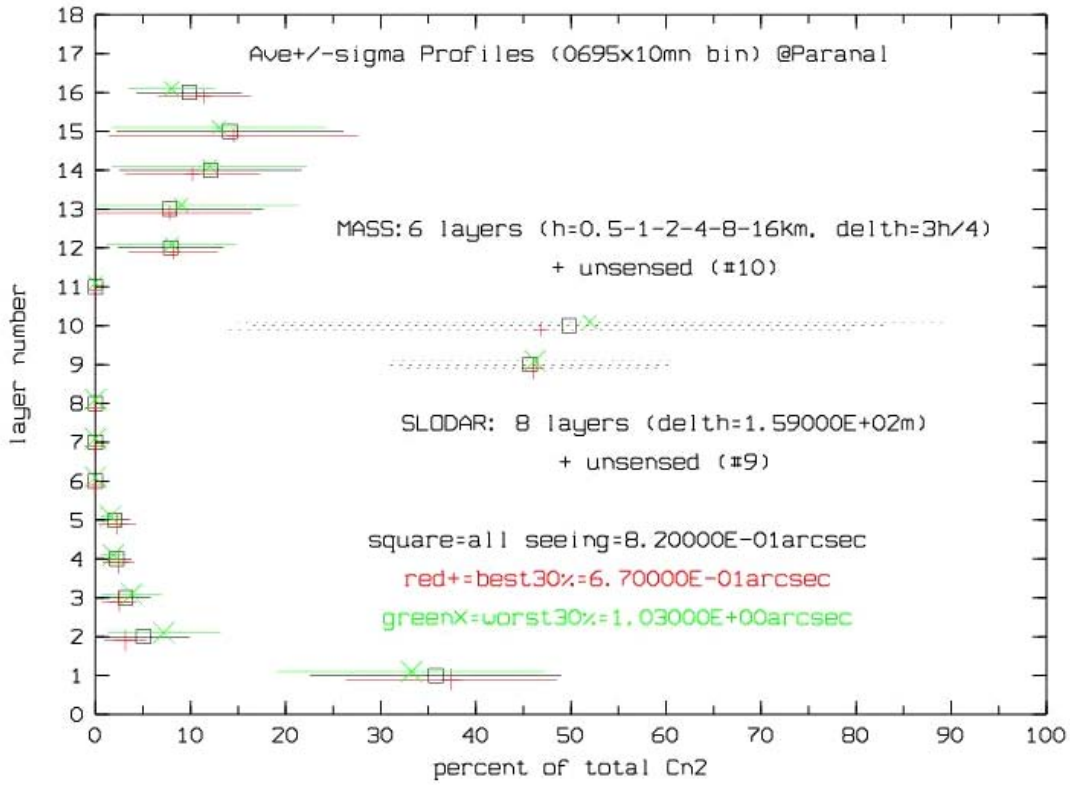

Figure 14-15: Relative contribution of the various atmospheric slabs to the integral of the turbulence obtained by combining SLODAR and MASS profiler data after reduction of the overlap area. The common database covers about 116 hours from February to August 2005.

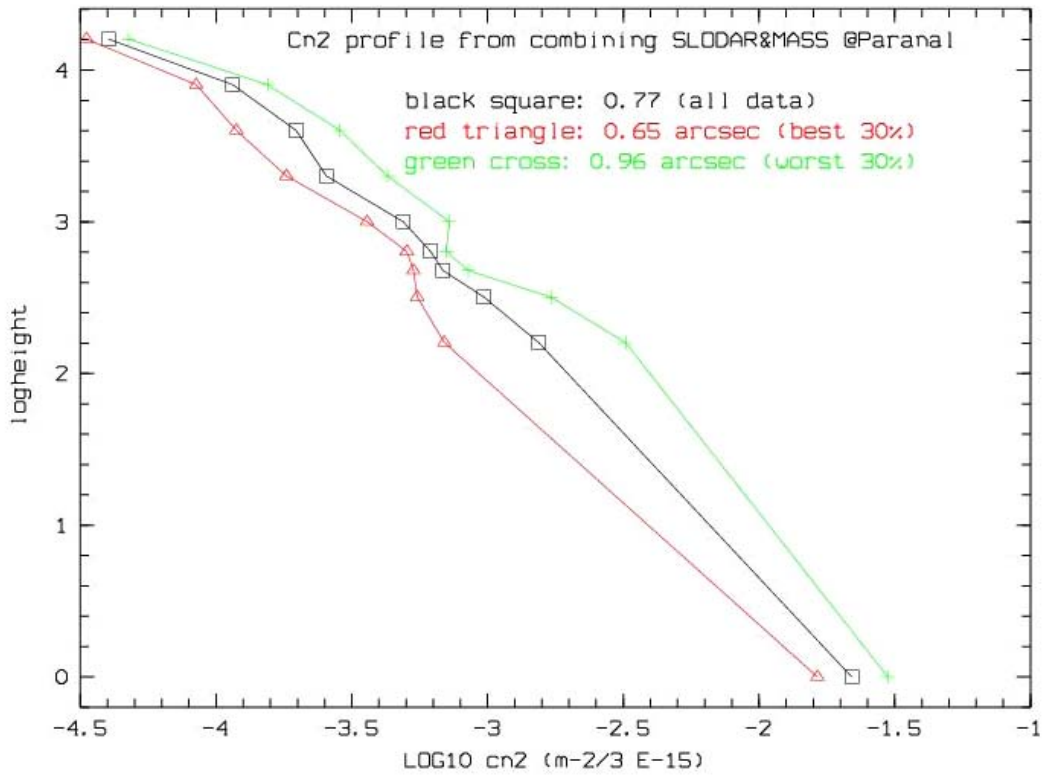

Figure 14-16: Complete atmospheric turbulence profile reconstructed from contemporaneous combined SLODAR and MASS measurements.

14.2.3.4 Sodium layer

The sodium layer considered here is situated in the mesosphere at 91.5±10 km and has a mean column density of $3x10^9 cm^{-2}$. This layer 'suffers' from seasonal. daily and short-term variations which are also strongly latitude dependent. The seasonal variations are 'sinusoidal' and affect the sodium column density. the average centroid position of the layer and its thickness. The sodium chemistry is known to be a sensitive function of temperature and the seasonal temperature variations appear to be largely responsible for the seasonal variations in the Na abundance which is maximal in winter (i.e. July-August in Chile). Measurements of sodium column density presently available for La Silla [114] show variations from 1 to $4.5x10^9$ cm^{-2}. Variations of the centroid position of the layer have a direct impact on the focus for laser guide star.

For Laser Guide Star Adaptive Optics. the short-term variations of the atmospheric sodium are the most worrisome. These variations can be classified in two types: the daily and 'hourly' ones.

Gravity waves are believed to be responsible for the daily modification of the Na layer. even though it is not yet clear how. These waves play an important role in the formation of sporadic Na layers (Nas). These are very thin (0.5 to 2 km thick) Na layers superposed to the mean mesospheric sodium layers. They are characterized by a rapid increase in sodium density over a narrow altitude range. They can last few seconds but in average few minutes up to few hours. The 'hourly' variations of the mesospheric sodium layer. mentioned above. are clearly dominated by these sporadic layers.

Sporadics have been detected more frequently at high and low latitude than mid-latitude sites. It has long been recognized that many Nas are associated with sporadic E layers. It has therefore been suggested that the apparition of these layers might be related to magnetic latitude more than to geographic latitude. Many groups have measured an enhancement of the sodium concentration during meteor showers. This can be understood since meteorite ablation is considered as the main source of mesospheric sodium.

Sporadics variations of the Na layers might be the most affecting effect for LGS AO. The coming LGS facilities at US and ESO observatories will clarify the relevancy of monitoring the sodium layer in the process of the site selection.

14.3 Site selection strategy

14.3.1 Identification of potential candidates

The site testing activity at ESO did not stop after choice of Paranal as the VLT site. In response to the tense situation about legal claims for land property. a one year site survey of an alternative site owned by the Max-Plank Institute was organized in Namibia in 1994-1995. The creation of Working Group on Alternative Sites was decided by Council during its April 19. 1995 meeting. with the task of proposing alternatives for the possible placement of one VLT telescope or the entire VLT/VLTI (ESO/Cou-549). It led to a detailed characterisation of Maidanak Observatory in Uzbekistan which ranks among the best for good seeing and low wind conditions [74]. This study was funded by the European INTAS program. The ESPAS (ESO Search for Potential Astronomical Sites) working group was revived after 2000. gathering specialists of climatology. turbulence modelling and atmospheric extinction. to prepare the site surveys for the next generation of optical telescopes. ESPAS gave a demonstration of what modern site characterization should be with a full assessment of Mauna Kea and a first climatological study of La Palma[72]. The emerging ELT projects in the U.S. also gave the opportunity of surveying the potential for the optical of Chajnantor [75]. where the ALMA project is currently being built. The TMT project currently conducts an ambitious site survey in Northern Chile. Mexico and Hawaii where automated stations have been deployed.

[72] http://www.eso.org/gen-fac/pubs/astclim/espas/espas_reports/

The long list of potential candidates for a European ELT was shortened in the frame of the ELT Design Study and the Site working group proposed to focus on the study of 4 sites shown on Figure 14-17 to Figure 14-20. keeping as a reference the recent results obtained at the newly operated Dome C Antarctic station.

Figure 14-17: Observatorio Roque de los Muchachos (ORM). La Palma. Canary Islands. Spain (http://www.otri.iac.es/sitesting/)

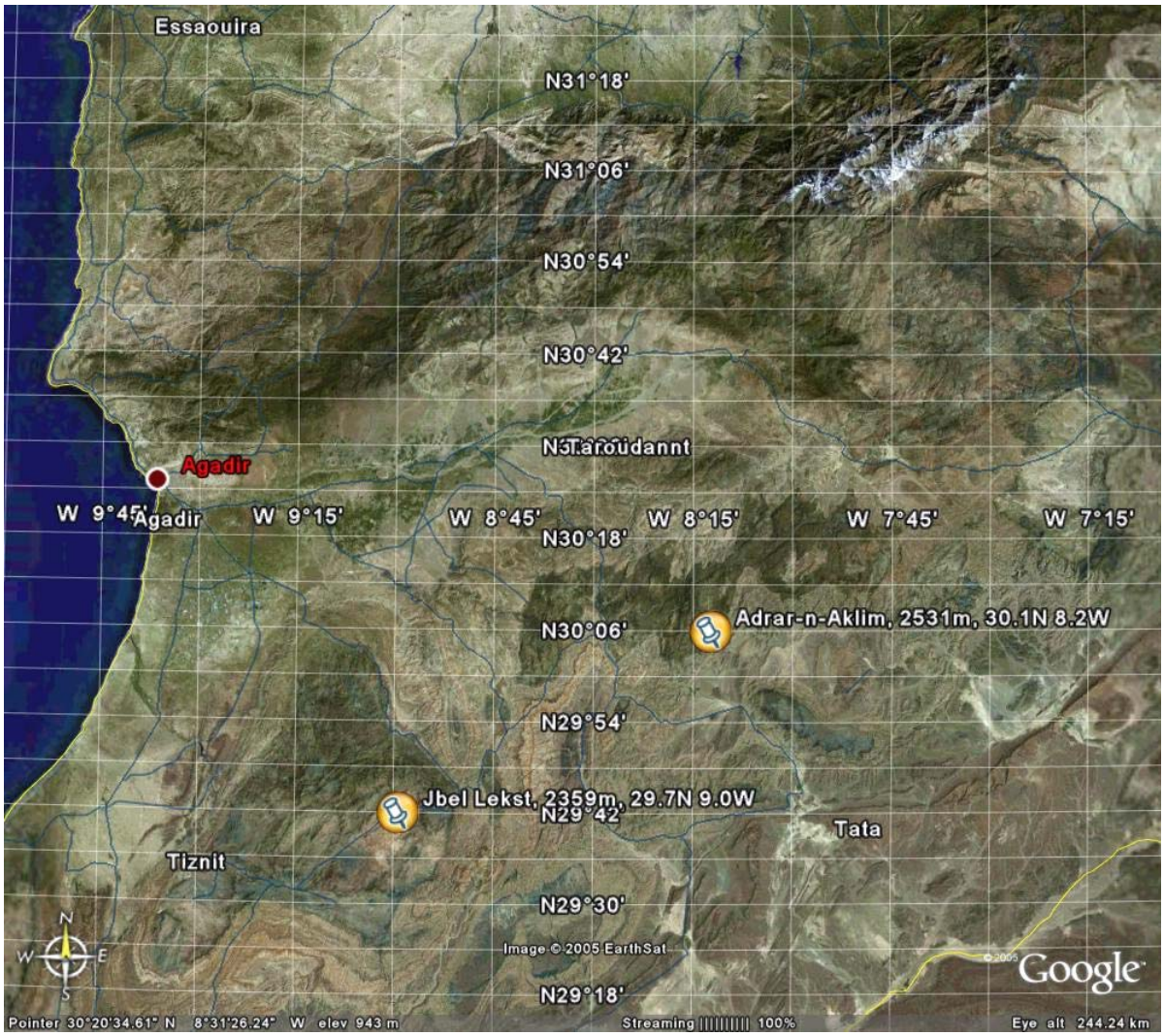

Figure 14-18: Morocco Anti-Atlas mountain area has the highest percentage of photometric nights along the North African continental west coast

Figure 14-19: Paranal North area proposes several candidate sites along what could become "the photon valley" of the 21st century

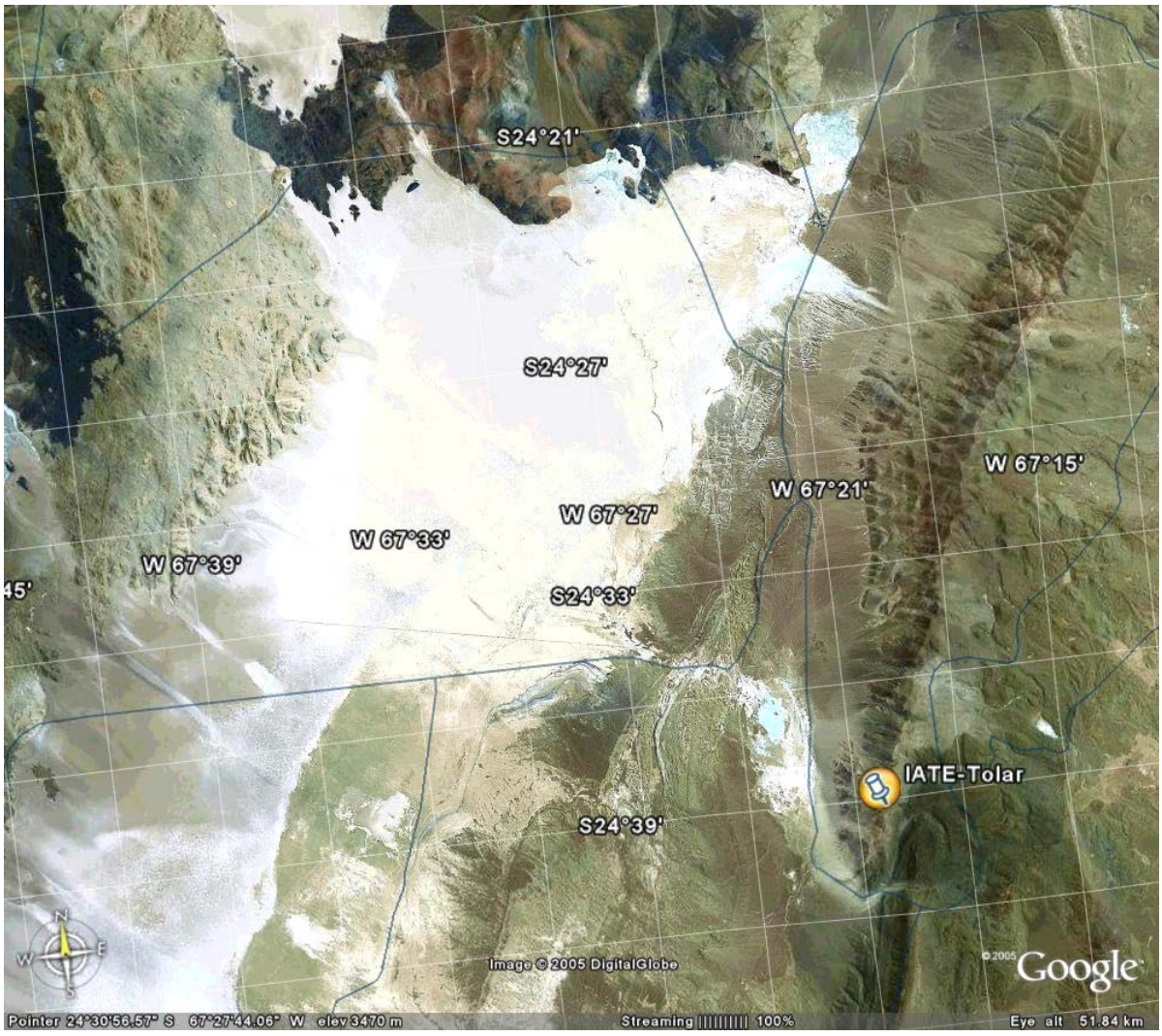

Figure 14-20: the Macon range. to the East of the huge Arizaro salt flat in NW Argentina allies high altitude (>4500m) and lower seismic activity (http://www.iate.oac.uncor.edu/tolar/)

14.3.2 Characterization of the parameter space

The OWL site characterization and the definition of figures of merit. as specified in section 2.9. should encompass. as a minimum. the following criteria (the ordering of the list below is not meant to reflect priorities):

1. Cloudiness;
2. Humidity. Precipitable Water Vapour;
3. Atmospheric Extinction;
4. Seeing or atmospheric coherence length;
5. Ground temperature. air temperature gradient and microthermal turbulence over the first 100 m;
6. Structure of the atmospheric turbulence. with a resolution not worse than +- 500 m in altitude up to ca. 20km;
7. Isoplanatic angle;
8. Turbulence coherence time;
9. Outer scale of the atmospheric turbulence;

10. Sodium layer density;
11. Wind speed and direction;
12. Precipitations (snow. rain. ice. fog);
13. Airborne aerosols. including dust chemical composition. particle size distribution and abrasive characteristics;
14. Site topology;
15. Soil properties. including typical stiffness.
16. Seismicity;
17. Survival loads (earthquakes. wind. precipitations);
18. Present and future potential light pollution; contrails;
19. Access to pre-existing infrastructures (roads. harbour. etc.); development costs;
20. To the foreseeable extent. long-term exposure to climate change;
21. To the foreseeable extent. potential long-term political stability.
22. Site-dependent operational costs.

14.3.3 Analysis of climate stability

14.3.3.1 The experience of ESO Observatory

It is not possible anymore. like it had been implicitly done during the VLT site survey. to consider any area of the world as climatically stable. The past climate. for sure was known to have been different [Grenon. 1990]. but on paleoclimatological scales much longer than a telescope lifetime. Indeed in the last decade. reports in the media. some of them very alarming. have shown that the equilibrium on which rests our current climate was very fragile. and also contained imbedded oscillations of various nature. Which of these oscillating meteorological parameters are relevant for the quality of astronomical observations? This is the object of an ongoing study using 20 years of cloudiness and seeing records at ESO Observatory (Figure 14-22 and Figure 14-23). aiming at finding links with well documented. although not yet predictable. events like such as El Nino Southern Oscillation Index (SOI) or the longer term Pacific Decadal Oscillation (PDO. Figure 14-21).

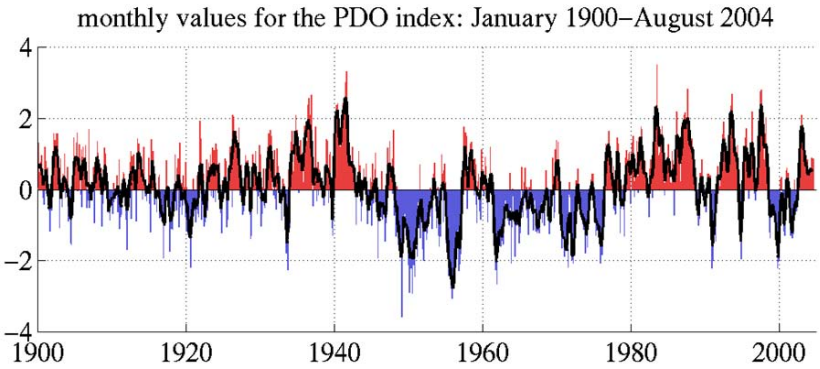

Figure 14-21: 20th century PDO "events" persisted for 20-to-30 years. while typical ENSO events persisted for 6 to 18 months

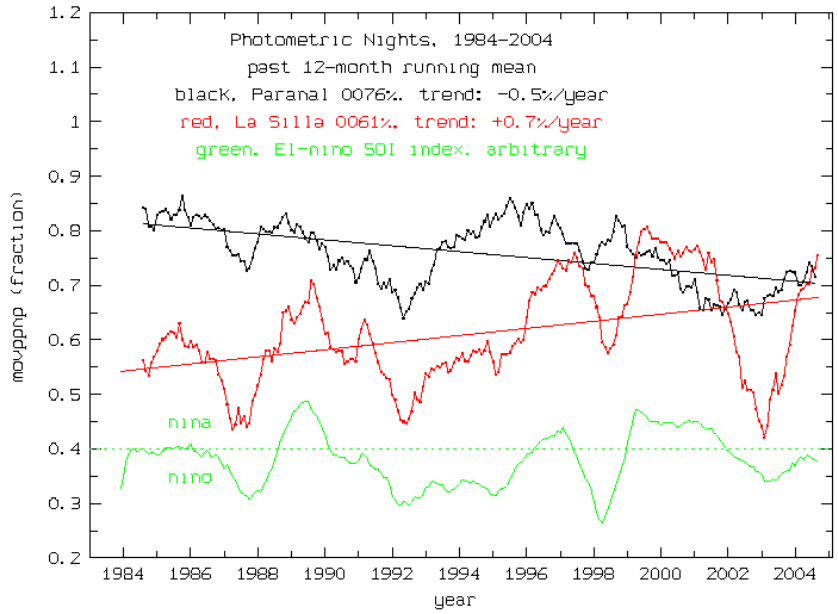

Figure 14-22: Monthly statistics of photometric nights at Paranal and La Silla and their relation to El-Nino Southern Oscillation Index

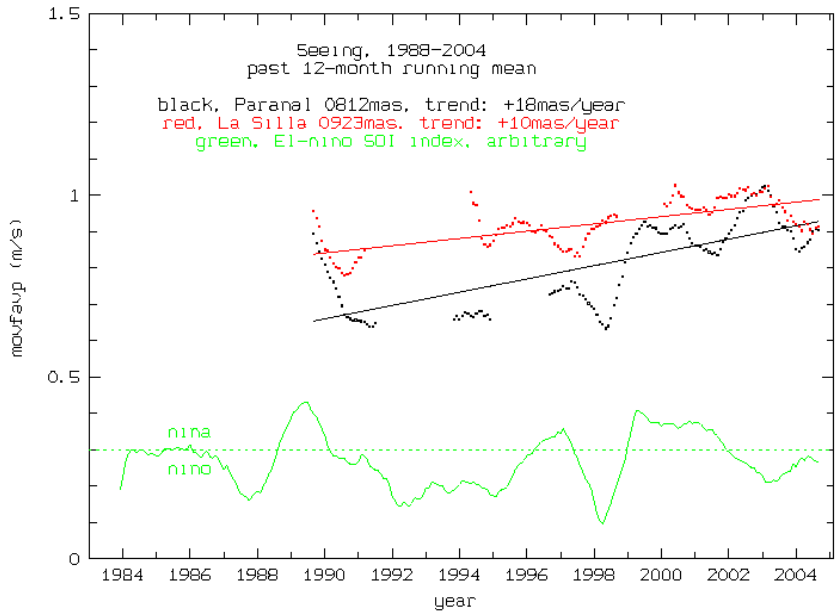

Figure 14-23: Monthly statistics of seeing at Paranal and La Silla and their relation to El-Nino Southern Oscillation Index

14.3.3.2 FRIOWL

For the most rigorous and best possible site selection process. a lengthy and detailed climatic database is needed. Added to this is the fact that global climate is changing and it will continue to do throughout the 21st century. An ideal site in today's climate may not prove ideal within 30 to 50 years. Therefore. future climate information (taken from the output of General Circulation Models) is also of great interest in the site selection process.

A composite database has been designed and built for the site selection task at the Department of Geosciences. University of Fribourg. The climatological database is mainly composed of ECMWF and NCEP-NCAR Reanalysis data at a global resolution of between 1° and 2.5°. Using

a Java computer language based interface. programmed in GIS fashion. all of this relevant information can be interrogated in order to find the best possible sites for the new telescope.

The historic climatological database is composed mainly of “Reanalysis” datasets from the European Centre for Medium Range Weather Forecasting (ECMWF) and the National Center for Environmental Protection / National Center for Atmospheric Research (NCEP-NCAR). A Reanalysis is a look backwards in time. re-creating the weather charts again for each time step in the past. but using the same climate model to do so.

600

Typically. both the ECMWF and NCEP-NCAR Reanalysis data have a global resolution of between 1° and 2.5° latitude / longitude. Although a resolution of 1° latitude still represents a distance of more than 100km on the ground. this is the best possible resolution available in current reanalysis projects. This resolution will probably increase with more advanced reanalysis projects in the future. Currently. the NCEP-NCAR Reanalysis project spans the period from 1948 to present (see http://www.cdc.noaa.gov/cdc/reanalysis/reanalysis.shtml for more information). The ECMWF Reanalysis project (ERA-15) spans a shorter period from 1979 to 1993 (http://www.ecmwf.int/research/era/ERA-15/index.html). although a new ERA-40 Reanalysis product is in the process of being made available from ECMWF. spanning the period from 1957 to 2001 (see http://www.ecmwf.int/research/era/). At a later stage of the OWL project. it is hoped to include the new improved ERA-40 dataset.

The full listing of meteorological and climatological parameters used in this study is given in Table 14-7 to Table 14-9. Of primary importance are variables such as cloud cover. atmospheric humidity. airflow direction and strength. aerosol content. and air temperature. Seismicity and topographic layers will be added to the database at a later time. Other secondary or computed variables (e.g. severe weather indices) may also be added.

File specification	Resolution	Period	File description
air2m.mon.mean.nc	T62 Gaussian grid (192 x 94 pts ~1.865°)	1948 – present	*Statistic:* air 2-metre temperature monthly mean. *Level:* 2m *Unit:* K
olr.mon.mean.nc	2.5°	1948 - present. but gap (1978)	*Statistic:* outgoing long wave radiation monthly mean. *Level:* other. *Unit:* not specified. probably W/m^2
pr_wtr.mon.mean.nc	2.5°	1948 - present	*Statistic:* monthly means of precipitable water vapour *Level:* integrated all levels as one. *Unit:* kg/m^2

Table 14-7: NCEP / NCAR Reanalysis datasets used

File specification	Resolution	Period	File description
Tcc	2.5° (144 by 73 grid points)	1979-1993	*Statistic*. total cloud cover [as a fraction between 0 and 1]. Fields of quantities accumulated over 24h periods centred on 12 UTC.
Surface	2.5° (144 by 73 grid points)	1979-1993	*Statistic:* U & V components of wind [m/s] at 10 metre level. Fields of quantities centred on 12 UTC.
850mb	2.5° (144 by 73 grid points)	1979-1993	*Statistic:* U & V components of wind [m/s] at 850mb level. Fields of quantities centred on 12 UTC.
200mb	2.5° (144 by 73 grid points)	1979-1993	*Statistic:* U & V components of Wind [m/s] at 200mb level. Fields of quantities centred on 12 UTC.

Table 14-8: ECMWF Reanalysis datasets used (ERA-15)

Air temperature (air2m) is provided by NCEP-NCAR as monthly means of 2-m air temperature from 1948 to present. Astronomical optics and engineering are sensitive to extremes of temperatures. so it may be necessary to include higher frequency air temperature datasets at a later stage of this project.

Outgoing Long wave Radiation (olr) is an indirect way of measuring cirrus clouds. which can be detrimental to astronomical viewing. Cirrus clouds strongly trap infra-red radiation. so negative anomalies of outgoing long wave radiation indicate a higher than normal presence of cirrus clouds. Large positive and negative anomalies of outgoing long wave radiation in the tropics are related to El Nino / La Nina weather patterns. which have been shown to affect astronomical viewing quality (*2*)

File name	Resolution	Period	File description
gmMMYY.n7a gmMMYY.epa	1.25° by 1.0° (288 by 180 grid points)	1978-1993 (Nimbus 7) 1996-1999 (Earth Probe)	Statistic: TOMS aerosol index as calculated from Nimbus-7 satellite (n7a) and Earth Probe (epa).

Table 14-9:TOMS Aerosol datasets used

Precipitable water vapour (pr_wtr) is provided as a monthly mean of integrated total column precipitable water vapour in kg/m^2 (which is equivalent to millimetres). It is the mean total amount of water that could be precipitated from the atmosphere. Values typically range from a few mm in cold regions to over 50mm in the tropics. An excellent site for OWL would be areas with a mean precipitable water content of less than 3mm throughout the year. In practice. such areas are only found in high altitude deserts or in the Antarctic.

Total cloud cover (tcc) information is provided by the ERA-15 dataset at a global resolution of 2.5° latitude / longitude. The data is calculated as the mean fraction of cloud cover (all levels) between 0 and 1. Cloud cover has obvious detrimental effects on astronomical viewing. blocking the incoming visible radiation. Preferential sites should have a cloud fraction of 0.1 or less.

Turbulence is a complex phenomenon. acting on many different scales. We will initially. however. investigate turbulence only at broad scales. such as that related to the jet stream winds. Therefore. daily wind direction and strength data has been obtained for the 200mb level from the ERA-15 period (1979-1993) at a grid resolution of 2.5°. Surface and 850mb level winds will also be included in the database in order to look at lower atmospheric effects.

Atmospheric aerosols also deteriorate astronomical viewing. as they can both absorb and scatter lights of different wavelengths. Therefore. Total Ozone Mapping Spectrometer (TOMS) aerosol data is been used in the OWL project database. The data is available from NASA[73] at a grid resolution of 1.25° by 1.0°. Due to the position of the TOMS satellite. however. data is only available for latitudes between 60° N and 60° S. It has been shown that TOMS aerosol index is related to aerosol optical depth and to atmospheric extinction.

A user-friendly web-based interface shown Figure 14-24 was designed at the University of Fribourg (Switzerland). It combines the ease-of-use of a GIS application. together with the climatological and geomorphologic database described above. There are several different operations that can be undertaken on the data and the maps displayed. Firstly. using the plus and minus buttons. the user can zoom into areas of interest on the chosen map. Secondly. he/she can choose different colour maps or palettes to display the maps. These colour maps are based on those provided by the software IDRISI Release 3.2 (*7*). Thirdly. he/she can choose an operation. These are simple mathematical operations performed on the selection of maps in your user-window. As of January 2004. the following operations are currently enabled on FRIOWL:

a) AVERAGE: the arithmetic average of all chosen user-maps is displayed

[73] see http://toms.gsfs.nasa.gov/aerosols/aerosols.html.

b) SUM: the arithmetic sum of all chosen user-maps is displayed

c) MAX: the maximum pixel value of all pixels of all chosen user-maps is displayed

d) MIN: the minimum pixel value of all pixels of all chosen user-maps is displayed

e) ANOMALY: this is a special feature; which displays the average of all certain selected maps. minus the average of all certain non-selected maps. In other words. it displays the mean of a set of maps. subtracted from the mean of another set of maps (i.e. the anomaly). You need to have a range of maps selected in the “Selected Files” window in order for this option to work.

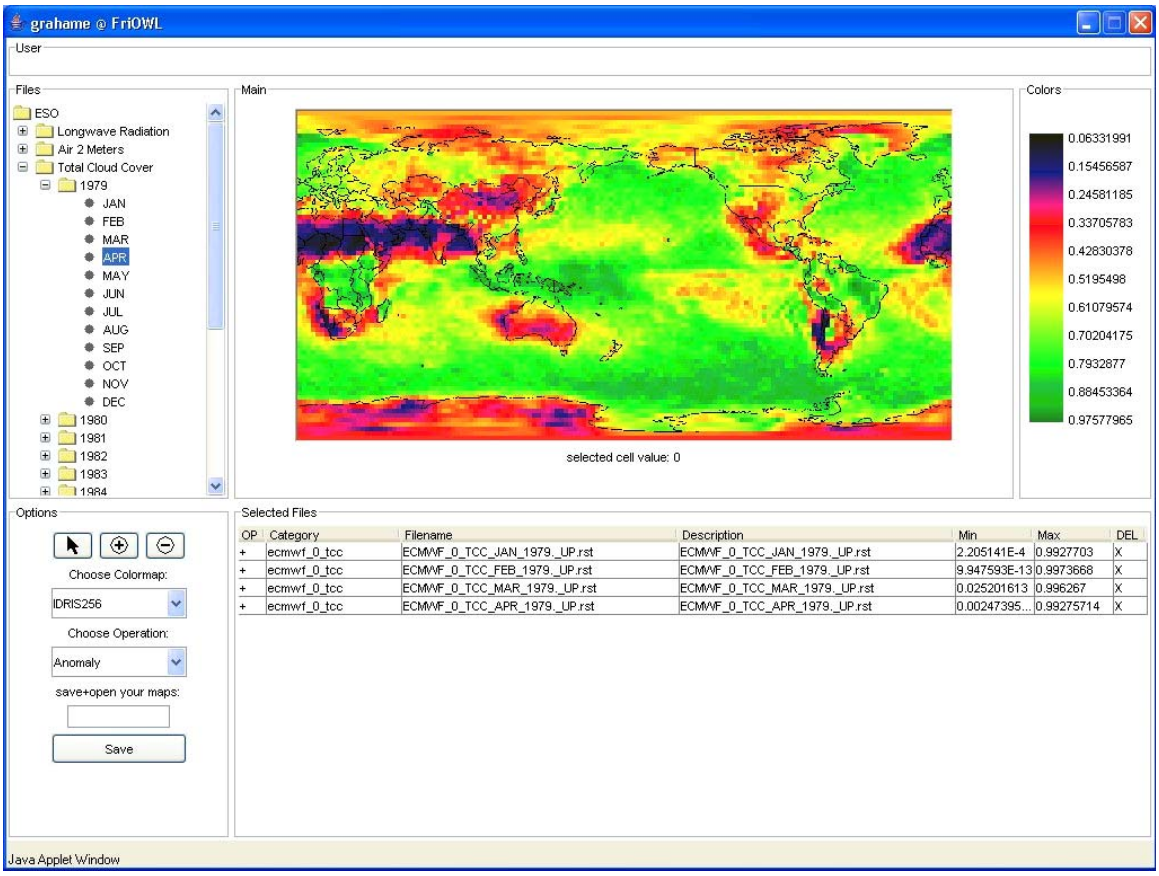

Figure 14-24: The FRIOWL user interface

14.4 Site preservation and monitoring

14.4.1 Local Seeing control

The measures taken at the VLT seem adequate for preserving the observing conditions inside and outside the enclosures. However an accurate estimate of the local contributions to the total image quality is very difficult to obtain. as discussed in the next section. In the case of OWL. the local thermal environment of the telescope shall receive a particular attention because the primary mirror lower edge can be close or even below ground when observing away from zenith. Obviously the local seeing conditions between the lower and the upper edge of M1 cannot be made equal but the differential seeing should be reduced as much as possible by a proper control of the ground temperature in the vicinity of the telescope.

It is important to develop a new generation of compact. cheap and easy to use seeing monitoring devices so as to adequately map the telescope 'observing volume' during operation (see next section). Maybe it will be considered interesting in this respect to attach a few such self-pointing devices on key locations like the rim of M1. or/and in the shadow of M2.

14.4.2 Astronomical Site Monitoring Station

Monitoring the astronomical observing conditions during the operation of the observatory has proven useful for increasing the observing efficiency in real time as well as for tracking long term changes. A typical monitoring station includes a meteorological station. seismic recorder. all sky monitor and seeing monitor. To these can be added if required single or double stars turbulence profilers.

It is important however to verify that the monitoring device. which has to be small and automated. is indeed picturing the actual environment of the ELT. A particular example is given by the seeing measurements using the DIMM (Differential Image Motion Monitor) at the VLT observatory. The seeing measured by the DIMM at 6 meter height above ground located at the northern edge of the VLT telescope area is used to characterise the expected image quality at the focus of the 8m unit telescopes as well as of the 1.8m auxiliary telescopes. A comparison with measurements obtained from the image quality at the focus of the active optics Shack-Hartmann lenslet array with 40cm diameter subapertures shows (Figure 14-25) that the distribution of both data sets is clearly different on the high range limit. The UTs. at seen from the active optics wave front sensor after correction for atmospheric dispersion. seem less sensitive to bad seeing than the DIMM would let believe. The comparison of two UTs on Figure 14-26 using a limited data set shows a good agreement in this respect although with a dispersion of 0.2 arcsec standard deviation. Thus one can deduce an improvement of the median seeing of the site. as seen by 10m class telescopes and larger. of about 0.15 arcsec in the visible. The reasons for the observed discrepancies are currently under study. One very satisfactory result is that UTs and DIMM agree very well in good seeing conditions. thus confirming that local conditions on the 8m mirror and inside the dome are very well controlled.

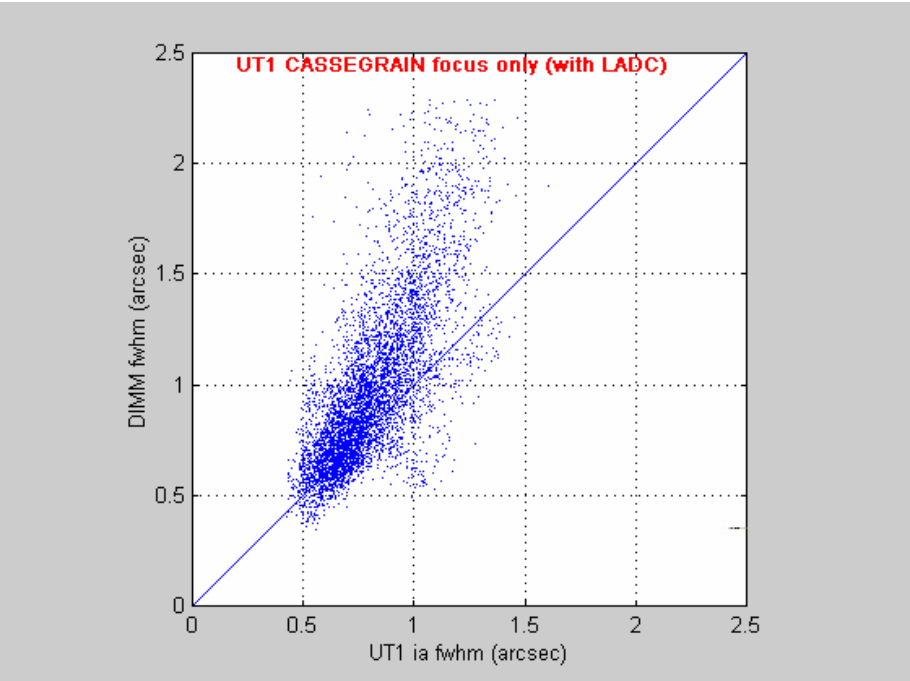

Figure 14-25: DIMM seeing (1mn average) versus contemporaneous UT1 Cassegrain Active Optics Image Quality (atmospheric dispersion corrected) estimates for January-August 2005 (compilation. J. Navarrete. Paranal).

The UT intrinsic focal plane seeing. as well as the final science image quality. is even more difficult to estimate from DIMM data. particularly in the infrared. because they have to be corrected from the finite nature of the outer scale of the turbulence. This correction improves the predicted large telescope image quality in a very chromatic manner [63]. This is well illustrated in Figure 14-27 which shows that fitting a 10m outer scale von-Karman correction to DIMM data is hardly sufficient to picture ISAAC IQ in bad seeing conditions. Moreover it would require a 0.3" local image degradation to explain the saturation during good seeing of the ISAAC IQ. Such local image degradation is not confirmed by active optics wave front sensor measurements of Figure 14-25. Discussion on the best outer scale modelling is still going on and a dedicated experiment is foreseen at Paranal in the frame of the ELT Design Study to actually measure the characteristics of wave fronts up to 50m in width

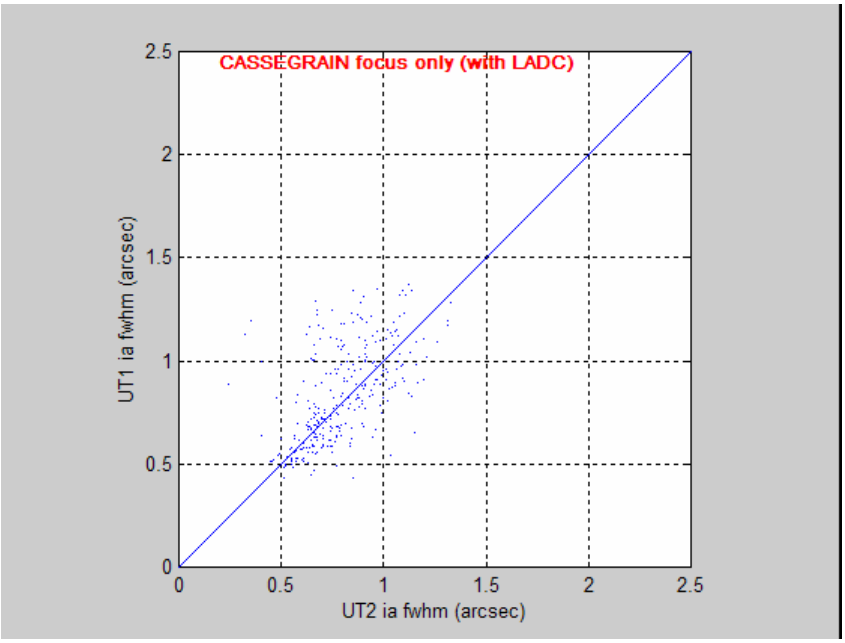

Figure 14-26: UT1-UT2 comparison of contemporaneous Cassegrain Active Optics Image Quality (atmospheric dispersion corrected) estimates for January-August 2005 (compilation. J. Navarrete. Paranal).

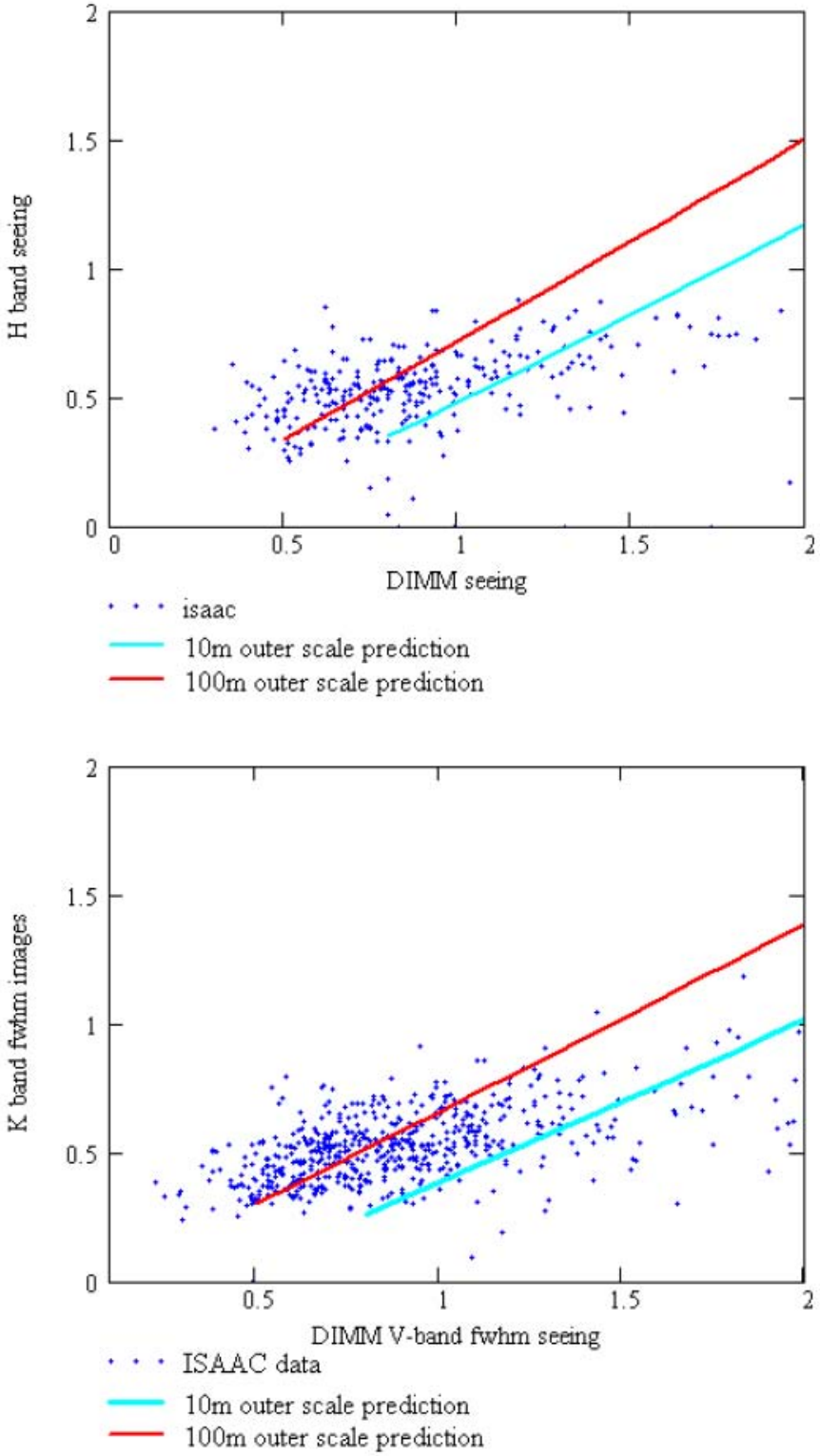

Figure 14-27: ISAAC. K (lower graph) and H (upper graph) band zenith image quality as measured (dots) and as exprected from DIMM after outer scale correction following [63]; M. Casali. I.R. image quality at the VLT. ESO Internal Report. 02 June 2005.